DYNAMIC STRESS CONCENTRATION DUE TO AN OBLATE SPHEROIDAL INHOMOGENEITY

Ratnam Paskaramoorthy
School of Mechanical Engineering, University of the Witwatersrand
Private Bag 3, Wits 2050, South Africa

ABSTRACT

The stress field around a spheroidal inhomogeneity is studied under dynamic loading condition with particular attention being focussed on the stress concentration due to the inhomogeneity. A hybrid method that combines the finite element methodology with an analytical approach has been used to solve the problem for an inhomogeneity in the form of an oblate spheroidal cavity. The results show that the dynamic stress concentration is influenced by the frequency of excitation, aspect ratio of the cavity and Poisson's ratio of the medium and that the dynamic stress concentration can be about 100% higher than that predicted for quasi-static loading.

KEYWORDS

Stress concentration, dynamic loads, inhomogeneity, elastic waves.

INTRODUCTION

Stress concentrations in elastic bodies arise in the presence of geometric and material discontinuities such as cavities, cracks, notches, inclusions, reinforcements, etc. Determination of stress concentration is a problem of considerable interest in many branches of applied mechanics since failure of a structural member often initiates at areas of high stress concentration. The review article of Sternberg (1958) presents a comprehensive survey of the literature under static loads. Stress concentration under dynamic loads has also been studied by many researchers. The excellent monograph by Pao and Mow (1973) gives comprehensive coverage on this and other related subjects. Recent results have been obtained by Bogan and Hinders (1993) for cylindrical geometries. A spheroidal geometry, however, presents considerably greater analytical and computational difficulties than does a cylindrical geometry.

In this paper the dynamic stress concentration around an oblate spheroidal cavity embedded in an infinite elastic medium is studied. The geometry of the problem is depicted in Fig. 1 where z-axis is the symmetry axis; $2a$ and $2b$ are diameters of the cavity along the x and z axes, respectively. The spheroidal cavity is said to be *prolate* for $b/a > 1$ and *oblate* for $b/a < 1$. The excitation of the medium is provided by a plane P wave propagating along the symmetry axis. The resulting stress field is axisymmetric. Only time-harmonic excitation is considered. Thus, all the field quantities have a time dependence $e^{-i\omega t}$, where ω is the frequency of excitation. The time dependence is suppressed in all subsequent representations for notational convenience. The problem is solved

by using a hybrid method that combines the finite element technique with spherical wave functions. In this approach, a fictitious spherical boundary B enclosing the cavity is drawn. The region interior to this boundary is modelled through an assemblage of conventional finite elements. The region exterior to the boundary B is represented by spherical wave functions. Coupling of these two different solutions is achieved by imposing the continuity of displacements and tractions along the common boundary B. This leads to a set of linear equations that enables determination of the displacements and stresses at any point of interest.

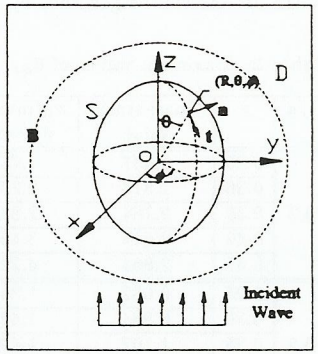

Figure 1: Schematic of the problem showing spherical coordinates

FORMULATION OF THE PROBLEM

The motion of the interior region may be perceived as forced vibration with the incident and scattered waves providing the forcing functions at the boundary B. The governing equations of motion can be obtained by following the conventional discretization process of the finite element methodology for axisymmetric elements, and are written as

$$[S]\{q\} = \{R\} \tag{1}$$

where

$$[S] = [K] - \omega^2[M] \tag{2}$$

in which $[K]$ and $[M]$ are, respectively, the stiffness and consistent mass matrices of the interior region; $\{q\}$ is the vector of nodal displacements; and $\{R\}$ is the vector of nodal loads that has non-zero components corresponding to the interface degrees of freedom only. If the vector $\{q\}$ is separated into two parts: $\{q_B\}$ corresponding to nodal displacement at the boundary B, and $\{q_I\}$ corresponding to nodal displacements elsewhere in the interior region, equation 1 can be written as

$$\begin{bmatrix} S_{II} & S_{IB} \\ S_{BI} & S_{BB} \end{bmatrix} \begin{Bmatrix} q_I \\ q_B \end{Bmatrix} = \begin{Bmatrix} 0 \\ R_B \end{Bmatrix} \tag{3}$$

in which R_B represents the interaction forces between the interior and exterior regions.

In the exterior region, the displacements and stresses are obtained from the superposition of incident and scattered wave fields which are denoted by the superscripts i and s respectively. Since the incident field is known, the vectors $\{q_B^i\}$ of nodal displacements and $\{R_B^i\}$ of nodal loads can be constructed by evaluating the displacements and stresses at each node lying on the boundary B. The scattered field is given by the wave potentials φ and ψ which can be expressed as an infinite series:

$$\varphi = \sum a_{1n} h_n(\alpha R) P_n(\cos\theta) \tag{4}$$

$$\chi = \sum a_{2n} h_n(\beta R) P_n(\cos\theta) \tag{5}$$

where all the summations are over integral values of n from zero to infinity; a_{1n} and a_{2n} are as yet unknown amplitude coefficients; R and θ are spherical coordinates; h_n is the spherical Hankel function of the first kind; P_n is the Legendre polynomial; α and β are wave numbers defined by:

$$\alpha^2 = \frac{\omega^2\rho}{(\lambda + 2\mu)} \quad ; \quad \beta^2 = \frac{\omega^2\rho}{\mu} \tag{6}$$

where λ and μ are Lame constants and ρ is the density of the medium. Each term in the series in equations 4 and 5 represents a spherical wave function. By considering a finite number of wave functions, it is possible to establish a relationship between the force and displacement vectors at the boundary B, as

$$\{R_B^s\} = [S_f]\{q_B^s\} \tag{7}$$

where the matrix $[S_f]$ is complex valued. The details of this development may be found in Paskaramoorthy *et al* (1988).

The global solution is obtained by invoking the continuity of displacement and stress components of the two regions at the nodes on the boundary B, leading to

$$\begin{bmatrix} S_{II} & S_{IB} \\ S_{BI} & S_{BB} - S_f \end{bmatrix} \begin{Bmatrix} q_I \\ q_B \end{Bmatrix} = \begin{Bmatrix} 0 \\ R_B^i - S_f q_B^i \end{Bmatrix}. \tag{8}$$

Once the above equation is solved for the nodal displacements, the field quantities at any point in the domain may be obtained.

NUMERICAL RESULTS AND DISCUSSION

In this study, excitation is provided by an incident P wave defined by

$$\mathbf{U}^i = \nabla\phi^i \quad ; \quad \phi^i = e^{i\alpha z} \tag{9}$$

which gives a maximum stress of $\sigma_o = \mu\beta^2$ in the absence of a cavity. In cavity problems, the primary interest is in the hoop stresses σ_{tt} and $\sigma_{\phi\phi}$ where $\mathbf{t}$ is the tangential vector to the surface of the cavity (Fig. 1). These stresses are expressed in dimensionless forms by normalizing with respect to the maximum stress, σ_o:

$$\overline{\sigma}_{tt} = \left.\frac{\sigma_{tt}}{\sigma_o}\right|_{R=a} \quad ; \quad \overline{\sigma}_{\phi\phi} = \left.\frac{\sigma_{\phi\phi}}{\sigma_o}\right|_{R=a} \tag{10}$$

Thus the values of the $\overline{\sigma}_{tt}$ and $\overline{\sigma}_{\phi\phi}$ can be considered as dynamic stress concentration factors. The stresses are computed for various frequencies from the nodal displacments of Eq. 8 by following standard finite element procedures. Since frequency of excitation is proportional to the wave number (Eq. 4), it is convenient to present the results for various values of dimensionless wave number αa.

In order to gauge the accuracy of the numerical procedure, we first consider the scattering by a spherical cavity which can be solved analytically. In Fig. 2, the numerical results obtained from the hybrid method are compared with the analytical solution for low ($\alpha a = 0.1$) and high frequencies ($\alpha a = 3$). It can be seen that the numerical results are in close agreement with the analytical solution.

Figure 3 illustrates the angular distribution of $\overline{\sigma}_{tt}$ and $\overline{\sigma}_{\phi\phi}$ for different values of αa. For $\alpha a = 0.02$, the frequency is very small and the wave length is approximately 150 times the

diameter of the cavity. At such wavelength, hardly any dynamic effects are present, and the dynamic solution can be regarded as representing a *quasi-static* solution. At other wave numbers, the scattering phenomena dominate, considerably distorting the results from the quasi-static solution.

The effect of normalized wave number αa on the dynamic stress concentration is illustrated in Fig. 4 by plotting the normalized stresses $\overline{\sigma}_{tt}$ and $\overline{\sigma}_{\phi\phi}$ at $\theta = \pi/2$ for different values of aspect ratio, b/a, and Poisson's ratio, ν. It can be seen that the Poisson's ratio of the medium significantly influences the results and that the dynamic stress concentration factors are higher than the quasi-static values. For instance, the peak value of $\overline{\sigma}_{tt}$ corresponding to $b/a = 0.2$ and $\nu = 0.45$ is about 48% higher than the quasi-static value. It is also noted that the dynamic amplification of stresses is more pronounced for smaller aspect ratios. This may be attributed to the sharp curvature at $\theta = \pi/2$. It is further noted that the dynamic amplification effects are more significant at low wave numbers indicating that a designer should be more concerned with low frequency than high frequency vibration.

Table 1 presents the maximum values of $\overline{\sigma}_{tt}$ in the wave number range 0.02–3.0 together with the maximum quasi-static values. It is not surprising that the maximum values are large when b/a is small since the cavity is approaching the geometry of a penny-shaped crack. The frequency and location at which maxima of $\overline{\sigma}_{tt}$ occurred are given in Table 1. It can be seen that $\overline{\sigma}_{tt}$ always reached its maxima at the point $\theta = \pi/2$. When the cavity is spherical, however, the maximum values occur at various locations. Finally, the percentage increase of the maximum dynamic stress concentration factor over the quasi-static value is given in the last column. This leads to the conclusion that the dynamic stress concentration factors are considerably larger than the quasi-static values. This becomes even more pronounced as Poisson's ratio increases.

Table 1: Maximum values of $\overline{\sigma}_{tt}$

b/a	ν	Quasi-static value	σ_{tt}(max) of dynamic	Wave number αa	location θ	Percent increase
0.2	0.25	6.379	8.336	0.78	90.00	31
	0.30	6.333	8.349	0.74	90.00	32
	0.35	6.266	8.412	0.69	90.00	34
	0.40	6.163	8.579	0.61	90.00	39
	0.45	5.965	8.977	0.49	90.00	50
0.5	0.25	2.987	3.512	0.68	90.00	18
	0.30	2.943	3.491	0.65	90.00	19
	0.35	2.882	3.485	0.62	90.00	21
	0.40	2.798	3.524	0.58	90.00	26
	0.45	2.669	3.748	0.52	90.00	40
1.0	0.25	1.848	2.000	0.55	88.00	8
	0.30	1.812	1.978	0.55	88.00	9
	0.35	1.764	1.974	0.60	86.00	12
	0.40	1.701	2.084	0.65	82.00	23
	0.45	1.616	2.616	0.56	66.00	62

In Table 2, the maximum values $\overline{\sigma}_{\phi\phi}$ are given. It can be seen that the percentage-increase values of $\overline{\sigma}_{\phi\phi}$ over quasi-static values are generally larger than those in Table 1. However, the absolute values of the maximum stresses (columns 3 and 4) are smaller than those in Table 1. Thus a design process will be governed by the stress $\overline{\sigma}_{tt}$.

Table 2: Maximum values of $\overline{\sigma}_{\phi\phi}$

b/a	ν	Quasi-static value	σ_{tt}(max) of dynamic	Wave number αa	location θ	Percent increase
0.2	0.25	1.437	1.781	0.79	90.00	24
	0.30	1.813	2.298	0.75	90.00	27
	0.35	2.184	2.845	0.70	90.00	30
	0.40	2.544	3.456	0.62	90.00	36
	0.45	2.864	4.221	0.49	90.00	47
0.5	0.25	0.682	1.349	3.00	0.00	98
	0.30	0.894	1.439	3.00	0.00	61
	0.35	1.107	1.492	3.00	0.00	35
	0.40	1.315	1.703	0.71	90.00	30
	0.45	1.502	2.260	0.60	90.00	50
1.0	0.25	0.544	0.997	2.75	0.00	83
	0.30	0.721	1.113	2.55	0.00	54
	0.35	0.907	1.281	2.27	0.00	41
	0.40	1.100	1.586	0.74	66.00	44
	0.45	1.300	2.457	0.60	24.00	89

CONCLUSIONS

The stress field and stress concentrations around a spheroidal cavity embedded in an elastic medium have been studied by using a hybrid method. The accuracy of the numerical method has been verified by comparison with analytical solutions for a spherical cavity. For a spheroidal cavity, it is shown that the dynamic stress concentration factors corresponding to the hoop stresses σ_{tt} and $\sigma_{\phi\phi}$ are significantly influenced by the frequency of excitation (or wave number), geometry of the cavity and Poisson's ratio of the medium. In general, the dynamic stress concentration factors are considerably higher than the quasi-static values, and in certain cases the percentage increase may reach as high as 100%. It is also found that the hoop stress σ_{tt} is more critical than the hoop stress $\sigma_{\phi\phi}$ for the problem at hand.

REFERENCES

Bogan, S. D. and Hinders, M. K. Dynamic stress concentrations in fiber-reinforced composites with interface layers. *J. Comp. Materials*, **27**, 1272–1240, 1993.

Pao, Y. H. and Mow, C. C. *Diffraction of Elastic Waves and Dynamic Stress Concentrations*, Crane and Russak, New York, 1973.

Paskaramoorthy, R., Datta, S. K. and Shah, A. H. Effect of interface layers on scattering of elastic waves. *J. Appl. Mech.* **55**, 871–878, 1988.

Sternberg, E. Three-dimensional stress concentrations in the theory of elasticity. *App. Mech. Rev.* **11**, 1–4, 1958.

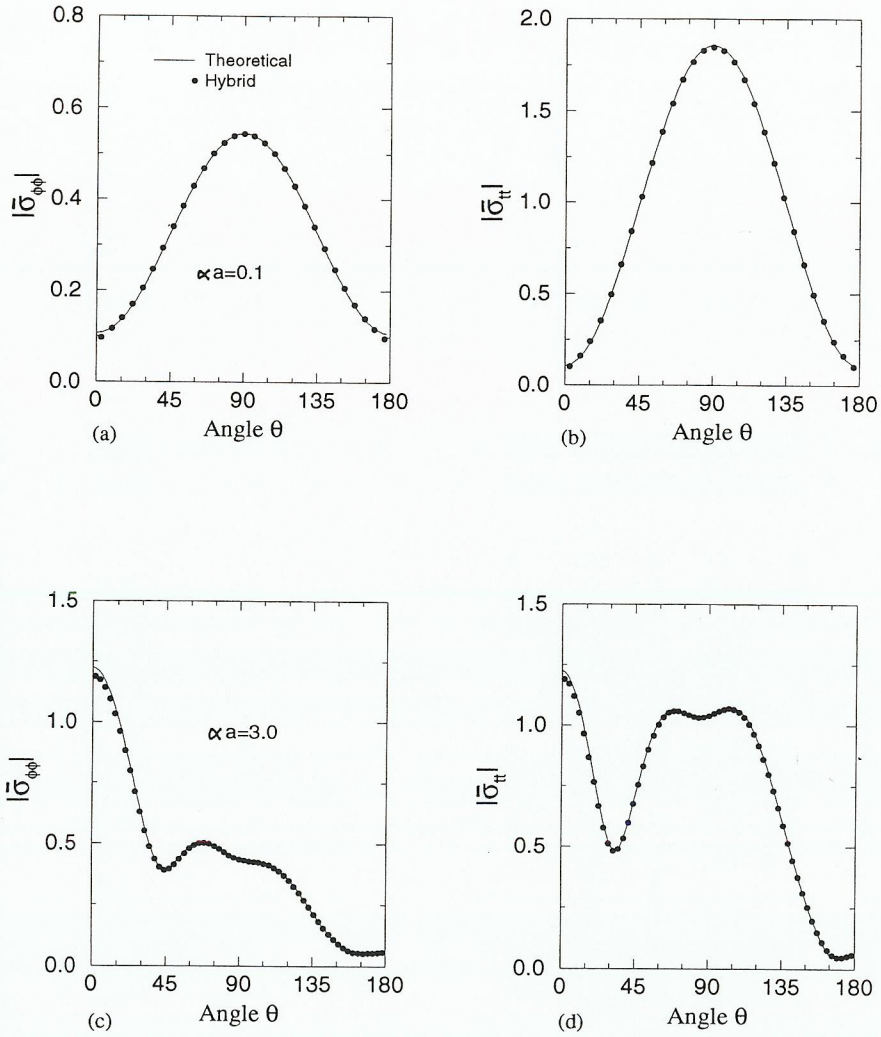

Figure 2: Comparison of stresses on the surface of a spherical cavity

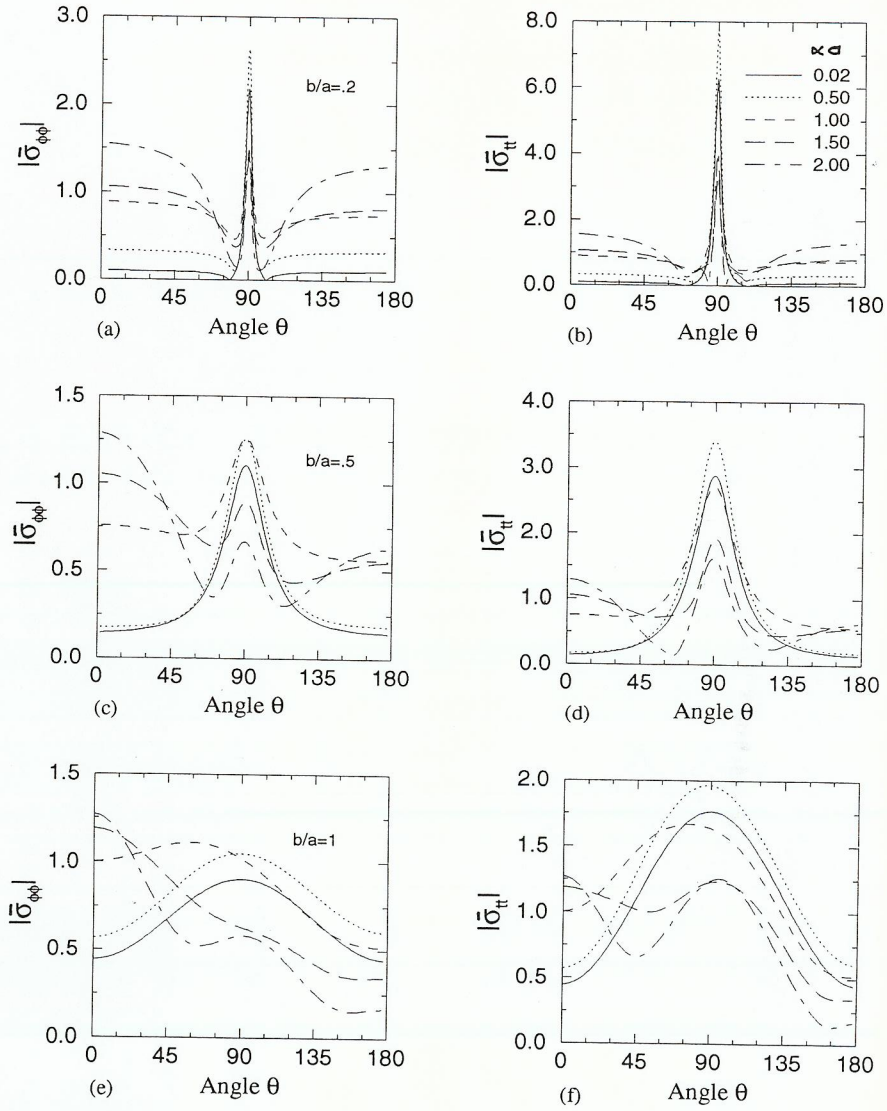

Figure 3: Angular distribution of stresses on the surface of the cavity (ν=0.35)

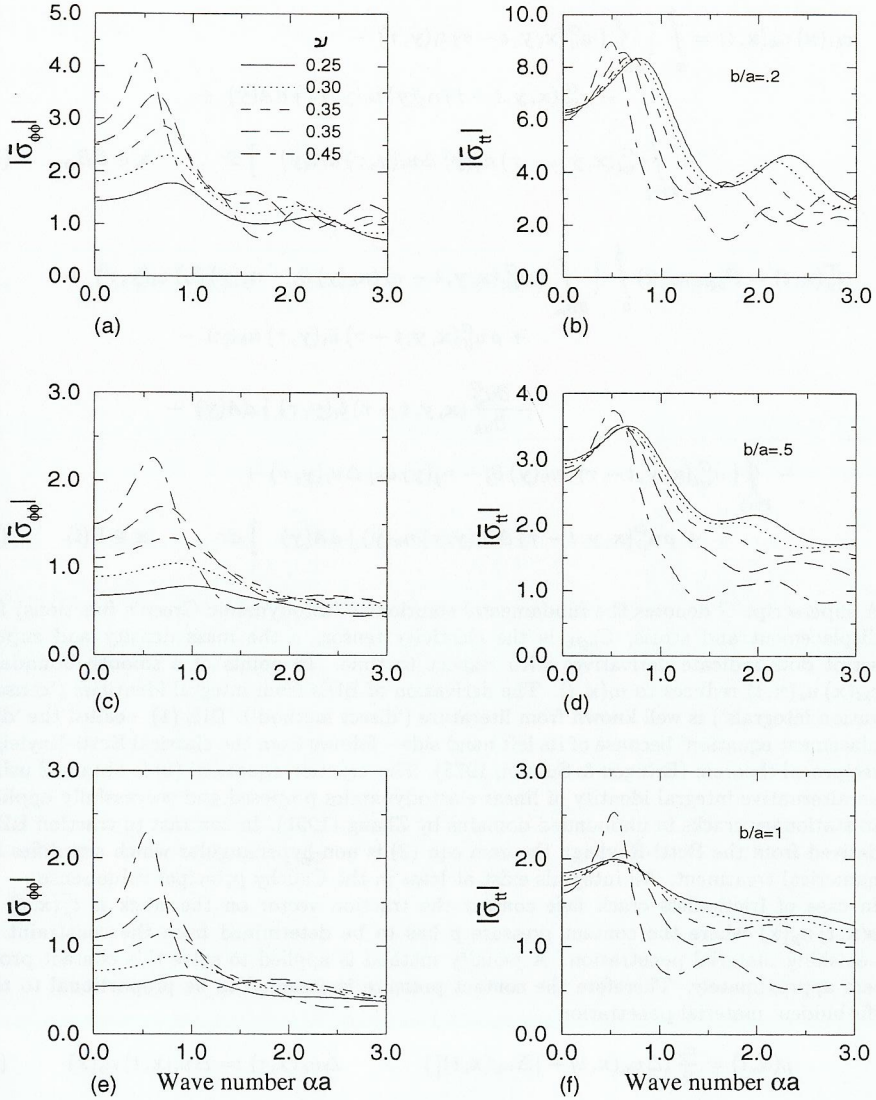

Figure 4: Effect of frequency on the stresses at $\theta=\pi/2$